

Quantitative Ultrastructural Studies of Hepatocytes from Fed and Starved Frogs

D. BAIC, B. G. LADEWSKI AND B. E. FRYE
Division of Biological Sciences, The University of Michigan,
Ann Arbor, Michigan 48109

ABSTRACT Stereological analysis of liver tissue excised from mature female *Rana pipiens* starved for 59 days and from a fed control group was conducted both at the light and electron microscopy levels. Average cellular volume decreased by more than a factor of 4 following prolonged fasting. Nuclear volume was not significantly decreased. Mitochondrial volume per cell showed a slight, though not statistically significant, decrease from $540 \mu\text{m}^3$ to $420 \mu\text{m}^3$. Rough endoplasmic reticulum decreased in absolute surface area per cell from $13,600 \mu\text{m}^2/\text{cell}$ to $3,000 \mu\text{m}^2/\text{cell}$ after starvation, but its surface density in the cytoplasm remained relatively constant. Lipid decreased from $650 \mu\text{m}^3$ per cell to less than $1 \mu\text{m}^3$ per cell after fasting. Glycogen decreased from 49% of hepatocyte cytoplasmic volume to less than 15%, a decrease in absolute volume from $4,000\text{-}240 \mu\text{m}^3$ per cell. Glycogen changed from the α to the β -configuration during fasting. Condensed cross-banded fibers or sheets formed within the rough endoplasmic reticulum cisternae of some fasted animals. The significance of these results relative to the energy metabolism of poikilotherms is discussed.

Biochemical and ultrastructural effects of glycogen-mobilizing stimuli on hepatic cells in mammals have been well-documented by a number of investigators (Cardell, '71; De Man and Blok, '66; Jones and Fawcett, '66; Kugler, '67; Magalhaes and Magalhaes, '70; Millonig and Porter, '60; Porter and Bruni, '60; Vrensen and Kuyper, '69). However, various biochemical findings suggest major differences in the physiology and biochemistry of liver glycogen mobilization in the frog compared to mammals. Liver glycogen levels can reach concentrations five to ten times higher than those typically found in mammals, while blood glucose levels are generally lower (Farrah, '72; Smith, '50). Smith ('50) for *Rana temporaria* and Mizell ('65) for *R. pipiens* observed marked seasonal variations in liver glycogen concentrations not directly related to availability of glycolytic substrate. Further, glycogen levels in frog hepatocytes are remarkably stable under starvation stress. Nicholls et al. ('68) reported that glycogen concentrations in the liver of *Xenopus laevis* were not significantly depleted by a 2-week starvation period and Spornitz ('75) found little change in ultrastructural organization or

density of glycogen particles in the same species even after four to five months inanition. Pasanen and Koskela ('74) observed substantial concentrations of liver glycogen in field-caught *R. temporaria* even after a 7- to 8-month wintering period.

The present investigation was undertaken to determine whether the above physiological and biochemical findings could be correlated with differences in frog hepatocyte ultrastructure and its glycogen reserves. The complete study involved comparison of the effects of various stimuli affecting glycogen deposition and mobilization, including glucagon and adrenalin treatments and extended periods of starvation followed by refeeding, on the ultrastructure of *R. pipiens* hepatocytes. The present paper deals with the first phase of the investigation: qualitative and quantitative determination of the normal ultrastructure of fed laboratory-confined *R. pipiens* during mid-summer. The base line morphology of fed animals was compared qualitatively and quantitatively with results obtained from animals maintained under similar conditions, but starved throughout the 59-day mid-summer period.

Investigators have described normal hepatocyte ultrastructure in several species of frog (Bennett and Glenn, '70; Bernhard, '69; Fawcett, '55; Spiegel and Spiegel, '70; Godula, '70; Spornitz, '75). Qualitative changes induced by artificial and natural stimuli such as natural metamorphosis (Bennett and Glenn, '70; Spiegel and Spiegel, '70), thyroxine-induced metamorphosis (Bennett et al., '70), and starvation (Duveau and Piery, '73; Spornitz, '75) have also been described for a small number of individuals from several different genera and species. However, although the effect of season on the extent of glycogen mobilization has been documented both biochemically (Mizell, '65; Pasanen and Koskela, '74; Smith, '50) and cytologically (Brachet, '69; De Robertis, '38; Ecker and Wiedersheim, '04) little work has been done in this area at the ultrastructural level. Our preliminary observations (Baic and Frye, unpublished data) indicated large corresponding seasonal variations in frog hepatocyte ultrastructure. These preliminary observations indicated a high degree of polarity in the subcellular organization within a given hepatocyte, a large variability in the cellular organization of adjacent hepatocytes, and an even greater variability in hepatocytes sampled from different individuals maintained under the same physical conditions. Such variability, even among adjacent cells within the same hepatic region, was also reported by Spornitz ('75) in *Xenopus laevis*. Brachet et al. ('71) observed similar heterogeneity in results derived from biochemical assays on "pools" of hepatic tissue from *Rana esculenta*.

The observed seasonal variations required establishment of a normal base line ultrastructure for each season of interest separately. The large variability found both within and between animals suggested that a base line established using quantitative stereological methods would be most useful in later experimental comparisons.

MATERIALS AND METHODS

Mature female *Rana pipiens* (weight approximately 40 gm) were selected for study. All animals used were obtained from the same southeastern Michigan supplier at the same time, in an attempt to reduce the large variability known to exist within natural *R. pipiens* populations (Farrar, '72). The frogs were given daily injections of tetracycline for 7 days after arrival in our laboratory (Nace et

al., '74) to counteract possible disease among the animals frequently brought on by their close confinement during shipping. All animals were then fed ad libitum for one week prior to initiation of the experiment.

Both experimental and control groups were housed in plastic cribs under controlled temperature ($21 \pm 2^\circ\text{C}$) and light (12:12 LD regime) conditions. Experimental treatments were initiated in mid-June and terminated in mid-August. Control animals were fed a diet of crickets ad libitum, supplemented occasionally with beef liver. Experimental animals were provided with water, but no food, throughout the 59-day experimental period.

Corresponding slices from the median distal lobe of the liver of each animal were excised for light and electron microscopic observation. The tissue was minced into 0.5-1.0 mm cubes and fixed using either (1) cacodylate-buffered glutaraldehyde-formaldehyde, pH 7.4 (Karnovsky, '65), followed by post-fixation in s-collidine-buffered osmium tetroxide, pH 7.4 (Bennett and Luft, '59), or (2) cacodylate-buffered KMnO_4 , pH 7.4 (Luft, '56). Samples were dehydrated through a graded ethanol series and embedded in Araldite. Both fixation procedures were carried out at 4°C . Only glutaraldehyde-osmium tetroxide fixed tissue was used in the quantitative analysis. Potassium permanganate was used as an alternate fixative since it fixes and stains glycogen but does not preserve RNA particles which may be mistaken for β -particles of glycogen (Millonig and Marinozzi, '68). Thin sections for electron microscopy ($\sim 700 \text{ \AA}$ thick) were contrasted with uranyl acetate and Reynolds' lead citrate and examined at $3,200 \times$ using a Phillips 300 electron microscope. Sections $1 \mu\text{m}$ thick were stained with toluidine blue for light microscopic observation and viewed using a Leitz Ortholux photomicroscope ($54 \times$ oil immersion objective).

Quantitative stereological methods

Two different levels of magnification were utilized in the quantitative stereological analyses. Large-scale parameters such as hepatocyte cell volume, nuclear diameter and hepatocyte volume density in the liver were investigated by light microscopy. Low power electron micrography was used for estimation of volume and surface densities of intracellular components.

To assure independence of samples obtained from consecutive grids in the electron micro-

graphic study, blocks were retrimmed after each grid of sections was cut. The first section scanned which filled the upper left corner of the grid square and which was not seriously damaged by sectioning or contamination artifacts was selected. Only one micrograph was taken from each grid of sections.

Electron micrographs were taken at $3,200 \times$ and enlarged to $12,700 \times$ final magnification on 11×14 photographic paper. Light micrographs were enlarged to $1,850 \times$. A 2.5-cm square sampling grid made of fine black thread was attached to the enlarging easel and superimposed photographically on the prints. Since several cellular components appeared to be anisotropic, two sets of measurements were made on each electron micrograph, using the horizontal and vertical lines of the sampling grid (Weibel and Bolender, '73).

Repeated magnification calibrations were made throughout the photographing and enlarging processes using micrographs of a replica grating. Including all sources of variation throughout the process, the coefficient of variation for electron micrograph magnifications was determined to be 2.5%.

Estimations of volume densities, i.e., the fractional volume of a component related to its containing volume, were made using linear integration (Rosiwal, 1898). The method is an extension of the Delesse principle which states that the areal density of profiles on sections is an unbiased estimate of the volume density of structures within the tissue (Delesse [1847] cited in [Weibel and Bolender, '73]), i.e.,

$$\frac{V_i}{V_T} = \frac{A_i}{A_T} = \frac{L_i}{L_T} \quad (1a)$$

Glycogen volume densities were determined using point counting (Glagoleff ['33] as cited in Weibel and Bolender ('73) and Chalkley ['43]), based on the further extension that

$$\frac{P_i}{P_T} = \frac{A_i}{A_T} \quad (1b)$$

(Notation and definitions are those of Weibel and Bolender ['73].)

Surface density, i.e., the surface area of a component per unit containing volume, was estimated using the method of Tomkeieff ('45) and Underwood ('68):

$$Sv_i = 2 \cdot \frac{I_i}{L_T} \quad (2)$$

where Sv_i = surface density of component i , I_i = number of intersections of the line probe with component i , and L_T = total line length

of the sampling probe. This formula was modified where appropriate to obtain the surface to volume ratio (R) of component i by dividing equation (2) by the volume fraction of component i (Loud, '68):

$$R_i = \frac{Sv_i}{V_{V_i}} = \frac{2 \cdot \frac{I_i}{L_T}}{\frac{L_i}{L_T}} = 2 \cdot \frac{I_i}{L_i} \quad (3)$$

where L_i = length of line traversing component i .

Numerical density of hepatocyte nuclei was calculated according to the formula derived by Floderus ('44) and Haug ('67) as cited in Loud ('68):

$$Nv_i = N_{A_i} / (\bar{D}_i - 2p_i + t) \quad (4)$$

where Nv_i = number of a given particle i per unit volume, N_A = number of profiles per unit area, \bar{D} = mean tangent diameter of particle i , p_i = perpendicular distance which the particle must penetrate into a section before it is visible, and t = section thickness. For light micrographs in this study, $t = 1 \mu\text{m}$. Since the smallest nuclear profile diameters observed were approximately $4.0 \mu\text{m}$ in diameter and the smallest diameter classes were assumed to be undervalued, an estimated value of $p_i = 0.55$ was utilized in nuclear density calculations. This value is slightly larger than the estimated value of $p_i = 0.3$ obtained by Loud ('68) for rat liver on sections of similar thickness. Hepatocyte nuclei were assumed to be spherical in shape; therefore, \bar{D} becomes simply the mean diameter of the population of spheres (Loud, '68). To obtain an estimate of \bar{D} from the distribution of cut-circle diameters (d_i), the Schwartz-Saltykov method of diameter analysis as outlined in Underwood ('70) was used. A second estimate of the parameter Nv_i was obtained from the Schwartz-Saltykov analysis.

Several assumptions are implicit in derivation of the quantitative formulae and the associated statistical analysis. Most of the stereological formulae assume a "two-dimensional" section; this assumption is never met in biological tissue, but is best satisfied in cases where the section thickness is small (i.e., < 0.10) relative to the diameter of components being measured (Weibel and Bolender, '73). Most statistical analyses performed assume normally distributed random variables with equal variances across experimental groups. These assumptions are rarely met in biological data, and the extent of deviation

from them is important in interpreting the significance of the quantitative results.

Statistical analyses were performed with the assistance of the MIDAS and BMD statistical packages available through the computing facilities at the University of Michigan. Parameter estimates are reported as the mean \pm 1 standard error, using a sample size of four animals for light micrograph calculations and three animals for electron micrograph analyses.

RESULTS

Light microscopy

Low power light micrographs of frog liver tissue (fig. 2) indicate a cellular organization that differs substantially from the lobular substructure observed in mammalian tissue. Repeated light micrographic observations on both paraffin and 1- μ m thick epoxy sections did not show a radiating pattern of sinusoids from the central vein, suggesting the absence of a distinct higher level of organization, such as a lobule substructure, within the network of frog hepatocytes (as was also reported by Ecker and Wiedersheim, '04; Spornitz, '75). The presence or absence of a lobular substructure within frog liver becomes significant when designing a sampling scheme for quantitative tissue analysis. Loud ('68) has shown that cells sampled from different regions of the liver lobule in rats show significant differences in volumes occupied by certain cytoplasmic components. Our light micrographic observations indicate that, if the lobular substructure exists at all within frog liver, it was not sufficiently well-defined in our samples to permit stratification of subsequent electron micrographic samples on the basis of sub-lobular location.

High power light micrographs of hepatocytes from the normal summer frog (fig. 3) indicate a cellular organization similar to that found by other investigators (De Robertis, '38; Fawcett, '55). Cells are polygonal, forming laminae at least two cells thick. Nuclei are nearly spherical, often located at the base of the cell, near the sinusoid. Lipid generally occurs adjacent to the sinusoids, while rough endoplasmic reticulum and associated mitochondria are found near the bile pole. The cytoplasmic ground matrix is light in density.

Two months starvation results in dramatic changes in hepatocyte morphology (fig. 4), in many respects similar to changes observed by Duveau and Piery ('73) in hepatocytes from

R. esculenta after eight months starvation. Sinusoids appear enlarged, hepatocytes greatly diminished in size. Cell polarity is no longer evident, with cytoplasmic organelles randomly scattered throughout the cytoplasm. Density of the cytoplasmic ground matrix varies considerably from hepatocyte to hepatocyte. Pigment cells are observed with greater frequency (arrow, fig. 4).

Table 1 summarizes results obtained from the quantitative light micrographic study. Quantitative estimations of mean nuclear diameter were made for starved and fed animals on 1- μ m thick sections using the Schwartz-Saltykov diameter analysis (figs. 1a,b). \bar{D} for control animals was calculated to be 8.6 μ m, for fasted animals 7.7 μ m. A two-sample t-test indicated no significant difference ($p > 0.05$) in nuclear diameter for experimental and control groups.

The number of nuclei per unit volume, N_V , was estimated using \bar{D} and Equation (4) above. Since N_V is less than 1, its reciprocal, $1/N_V$, has been reported instead. If the existence of binucleate cells is ignored, $1/N_V$ is an estimate of the volume per unit nucleus, i.e., the cellular volume (Loud, '68). Since few binucleate cells were observed during this or subsequent studies, and since binucleate cells in other species appear to have approximately twice the volume of mononucleate cells (Elias, '55; Loud, '68), $1/N_V$ is a reasonable first approximation for total cellular volume. A second estimate of $1/N_V$ obtained using the Schwartz-Saltykov diameter analysis is also presented in table 1. Average cytoplasmic volume was calculated as $1/N_V$ minus the average nuclear volume, i.e., 8,200 μ m³ for control animals, 1,600 μ m³ for fasted.

The nuclear surface to volume ratio was calculated independently of the nuclear diameters obtained above, using Equation (3). The surface to volume ratio determined for control animals was 0.67 μ m⁻¹, for fasted 0.74 μ m⁻¹. A comparison of these numbers with the theoretical values based on an assumption of spherical shape and a nuclear diameter as calculated above indicates a high degree of consistency in the data.

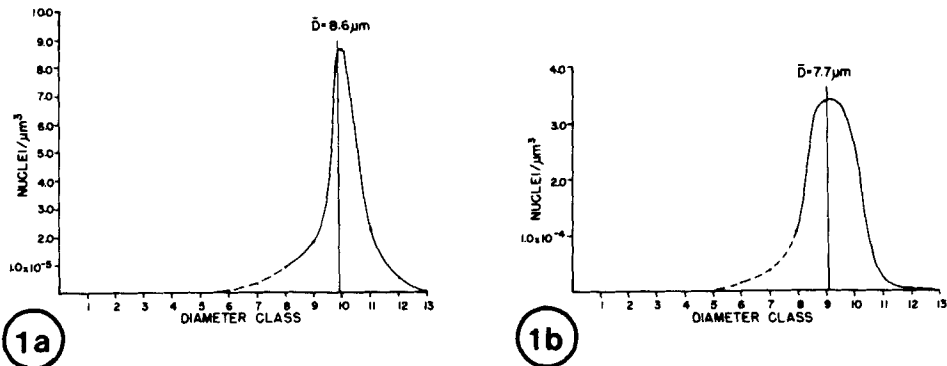
$$R_{\text{theor}} = \frac{4\pi r^2}{\frac{4}{3}\pi r^3} = \frac{3}{r} \quad (5)$$

For control animals, $R_{\text{theor}} = 0.70$; for starved, $R_{\text{theor}} = 0.78$. These estimates correspond well with those derived from Equation (3), and

TABLE 1

Summary of quantitative light micrographic results

	Control	Fasted	Sig. level ⁴
Number of animals examined	4	4	
Total number of light micrographs	8	8	
Total hepatocyte area examined (μm^2)	93,200	71,600	
Number nuclei counted	91	306	
Average nuclear diameter (μm) ¹	8.6 (± 0.41)	7.7 (± 0.42)	NS
Nuclear volume (μm^3)	340	240	—
Nuclear surface/volume ratio (μm^{-1}) ²	0.67 (± 0.03)	0.74 (± 0.02)	NS
Average cellular volume (μm^3) ¹	7,000	1,300	—
Average cellular volume (μm^3) ³	8,500 ($\pm 1,800$)	1,800 (± 250)	*
Average cytoplasmic volume/cell (μm^3) ³	8,200 ($\pm 1,800$)	1,600 (± 250)	*
Nuclear/cellular volume percent	4.3% (± 0.8)	16.5% (± 1.5)	*
Hepatocyte/tissue volume percent	80.3% (± 4.1)	61.7% (± 3.3)	*

¹ Calculated using Schwartz-Saltykov diameter analysis.² Calculated independently of estimated nuclear diameter.³ Calculated using Floderus-Haug equation.⁴ Differences between means tested using two-sample t-test, or Cochran's approximation for the Behren's-Fisher test (Snedecor, '56) when variances unequal. * = sig at 0.05 level.Fig. 1 Distribution of nuclear diameters for (a) control and (b) fasted animals as determined by the Schwartz-Saltykov diameter analysis on circular profiles. \bar{D} = mean nuclear diameter.

indicate that the assumption of nuclear sphericity is consistent with the data.

Electron microscopy

The findings of Fawcett ('55) on frog liver ultrastructure agree with our general observations on fed animals from late summer, i.e., the common occurrence of lipid, granular endoplasmic reticulum frequently in stacks of broad flat vesicles, and mitochondria in the form of plump rods or short filaments, with particularly simple internal structure.

The polarity discussed above in relation to

light micrographs is also evident in low power electron micrographs (figs. 5, 6). Large lipid droplets generally occur in high concentrations near cell boundaries bordering on the sinusoids; rough endoplasmic reticulum and associated mitochondria tend to cluster either around the nucleus or at the bile pole (fig. 6). Agranular endoplasmic reticulum is not abundant. It tends to occur at the periphery of large "glycogen areas," generally located between the glycogen deposits and clusters of granular endoplasmic reticulum and mitochondria, and is often continuous with the

granular phase (fig. 7). Mitochondria occur in many different shapes and sizes, but long thin filaments are the most frequently observed form.

Three different morphological forms of glycogen were observed in control animals throughout the study (figs. 5-9), and were similar to the various forms described by other investigators (Karrer, '61; Minio et al., '66; Vye and Fischman, '71). Although Revel ('64) described the state of aggregation of amphibian glycogen as the β configuration, our results indicate that aggregates similar to α -rosettes (as defined by Drochmans, '62; Revel, '64) also occur (fig. 9). These aggregates have a diameter ranging from 100-130 μ m, somewhat smaller than α -rosettes observed in rats (reported to be 150-200 μ m in diameter by Drochmans ['62] and Revel ['64]).

Vye and Fischman ('71) reproduced the different "morphological forms" of glycogen by utilizing different glycogen stains on tissue previously fixed in glutaraldehyde and post-fixed in osmium tetroxide solutions. They observed highly-variable glycogen staining from lead solutions, even from the same lead preparation, and uranyl acetate-lead citrate staining produced amorphous hyaline areas in regions of expected glycogen deposits similar to those observed in our tissue. Therefore it appears that the various glycogen densities and forms observed are a function of the staining technique and not of the quality of fixation. In the apparently empty "glycogen areas" in our tissue, we were able to resolve at higher magnification interconnected globular fragments of glycogen (fig. 8), also observed by Vye and Fischman ('71).

Most cellular structures exhibit significant morphologic changes following the 2-month fasting period. Mitochondria appear swollen, often assuming spherical or slightly oval shapes (fig. 11). Figures 10 and 11, permanganate-fixed tissue from summer fed and fasted frogs photographed at the same magnifications, illustrate the dramatic changes in mitochondrial shape observed after fasting. Nuclei occasionally show significant deviations from a circular or elliptical form. A significant decrease also occurs in the quantity and size of lipid droplets and the quantity of glycogen within the cell. The polarity of intracellular components observed in fed summer frogs is no longer evident after fasting (figs. 12, 13). Previously observed stacks of granular endoplasmic reticulum are conspicuously absent;

small vesicles with varying numbers of attached ribosomes and short segments of granular endoplasmic reticulum are scattered throughout the cytoplasm (fig. 12). Smooth endoplasmic reticulum does not appear to proliferate during starvation. However, segments of rough endoplasmic reticulum appear devoid of ribosomes and free ribosomes can be observed scattered in the cytoplasm near vesicles of rough endoplasmic reticulum (fig. 14 at arrows). Lightly-stained particles surrounded by clear cytoplasmic areas probably correspond to glycogen, although they appear smaller and more irregular in shape and are much less densely packed in the cytoplasm than glycogen particles in fed animals. (Compare figs. 9 and 15).

Electron dense material, either amorphous or condensed into cross-banded fibers or sheets (previously reported by Baic et al., '73), was occasionally observed in cisternae of the rough endoplasmic reticulum in fasted animals from various seasons (figs. 16 and 17 at arrows). The frequency of occurrence of such inclusions varied greatly from season to season, from animal to animal and even from cell to cell within the same animal. Evidence of organelle degeneration and intracellular digestion was also observed in hepatocytes of fasted animals. Accumulation of electron dense material was frequently seen in the cytoplasm, in its advanced stages generally associated with a break-down in organelle structure (fig. 13). Membrane-bound vesicles containing cellular organelles in various stages of degradation were also occasionally observed in fasted cells (fig. 18).

Quantitative results obtained from the electron micrographic study are summarized in table 2. Cytoplasmic volume fractions were obtained using the linear integration method described above. Total volumes were calculated as the product of the appropriate volume fraction and the cytoplasmic volume obtained above (Floderus-Haug calculation) in the light micrographic analysis. Standard errors of total volumes were calculated as a worst case approximation using the formula for $\text{var}(x \cdot y)$; therefore, t-test results are not presented for these quantities. Mitochondrial surface-to-volume ratios were calculated using Equation (3) above; rough endoplasmic reticulum and mitochondrial surface densities were obtained from Equation (2).

A pilot survey of mitochondrial axial ratios indicated that fasting substantially altered

TABLE 2

Summary of quantitative electron micrographic results

	Control	Fasted	Sig. level ¹
Number of animals examined	3	3	
Total micrographs counted	48	48	
Total area cytoplasm scanned (μm^2)	6,970	5,420	
Total intersections counted			
Mitochondrial envelope	1,778	3,649	
Rough endoplasmic reticulum	4,573	3,440	
Percent of cytoplasm			
Mitochondria	6.6%	25.9%	*
	(± 1.9)	(± 2.8)	
Lipid	7.9	0.01	*
	(± 1.5)	(± 0.01)	
"Glycogen areas"	48.8	14.9	*
	(± 2.9)	(± 5.6)	
Other	0.16	0.94	*
	(± 0.08)	(± 0.15)	
Absolute volume (μm^3)/cell			
Mitochondria	540	420	—
	(± 240)	(± 95)	
Lipid	650	0.13	—
	(± 230)	(± 0.14)	
"Glycogen areas"	4,000	240	—
	($\pm 1,000$)	(± 110)	
Other	15	15	—
	(± 8)	(± 4)	
Mitochondrial surface/volume ratio (μm^{-1})	7.0	5.2	NS
	(± 0.8)	(± 0.6)	
Mitochondrial outer envelope surface density (μm^{-1})	0.43	1.3	*
	(± 0.08)	(± 0.06)	
Rough endoplasmic reticulum surface density (μm^{-1})	1.7	1.9	NS
	(± 0.1)	(± 0.05)	
Absolute surface areas (μm^2)/cell			
Mitochondrial outer envelope	3,600	2,100	—
	(+1,250)	(+390)	
Rough endoplasmic reticulum	13,600	3,000	—
	(+3,600)	(+520)	

¹ Differences between means tested using two-sample t-test, or Cochran's approximation for the Behren's-Fisher test (Snedecor, '56) when variances unequal: *, Sig. at 0.05 level.

mitochondrial shape. However, a wide range of shapes (e.g., fig. 14), particularly in control animals, made it impossible to postulate either a consistent geometric shape or a constant axial ratio for the mitochondria. Since such assumptions are necessary to obtain estimations of number per unit volume, it was not possible to determine whether changes in the actual number of mitochondria per cell occurred under the stimulus of fasting.

Although the assumption is generally made that mitochondria are cylindrical in shape, our axial ratio data (table 3) indicate this assumption may not be appropriate for normal summer frogs. For infinitely long circular cylinders Elias et al. ('54) reported the theoretical percentages of randomly-sectioned two-dimensional profiles with axial ratios of 1-2, 2-4, 4-8 and 8- ∞ (table 3). A Chi-square

TABLE 3

Mitochondrial axial ratios

	Control	Fasted	Theoretical ¹
Number of mitochondria examined	735	1,007	—
Percent of profiles with axial ratio:			
1-2	63 (± 4.1)	85 (± 3.7)	86.6
2-4	21 (± 3.4)	11 (± 2.0)	10.2
4-8	11 (± 1.2)	4 (± 1.7)	2.4
8- ∞	4 (± 0.9)	0.5 (± 0.3)	0.8

¹ Based on data from Elias et al. ('54) for infinitely long circular cylinders.

test comparing observed and expected frequencies of mitochondrial profiles falling into these four categories indicated a very significant deviation from the model ($P < 0.0001$)

for control animals in our study. Fasted animals were also found to differ significantly from the circular cylinder model ($P < 0.05$). Both control and fasted animals exhibited higher frequencies than expected in the larger axial ratio categories.

Glycogen measurements included the clear rings which generally surrounded both α - and β -particles (as suggested by Loud [68]), but did not include the membranous component scattered throughout the glycogen areas. No selective staining procedure was used to identify cellular inclusions such as lysosomes or microbodies. Therefore cellular inclusions which included organelles morphologically similar to lysosomes and microbodies were combined into a single category labelled "Other." The volume represented by this category was so small that the present sampling scheme could not accurately determine its volume fraction in the cytoplasm. The combined group appears to be less than 1% of the total cytoplasmic volume.

Intersections of the sampling lines with portions of granular endoplasmic reticulum were recorded only if ribosomes were clearly attached to the membrane on both sides of the point of intersection. Loud (68) has suggested that intersection counts of random membranes should be increased by 50% to correct for membranes sectioned at an angle greater than 60° . This correction was applied to the surface densities reported for rough endoplasmic reticulum in table 2. The surface densities—1.7 and $1.9 \mu\text{m}^2$ per μm^3 tissue for control and fasted animals respectively—represented the surface area of rough endoplasmic reticulum facing the cytoplasm. No attempt was made to estimate the surface density of smooth endoplasmic reticulum, since ambiguities associated with glycogen identification and the nature of the cytoplasmic ground matrix made it difficult to clearly distinguish vesicles of smooth endoplasmic reticulum. Absolute membrane surface areas per cell were calculated as the product of membrane surface density times cytoplasmic volume for both rough endoplasmic reticulum and the outer mitochondrial envelope.

DISCUSSION

The quantitative light and electron microscopic observations presented here for normal *R. pipiens* are similar to results previously reported in the literature for *Xenopus laevis* (Godula, '70). Using slightly different mor-

phometric methods, Godula calculated average cytoplasmic hepatocyte volume for normal *X. laevis* to be $7,435 \mu\text{m}^3$, compared to $8,200 \mu\text{m}^3$ reported here for *R. pipiens* control animals. The nuclear/cellular volume fraction for *X. laevis* as calculated from Godula's data was 2.6%, lipid/cytoplasmic fraction 1.2%, and mitochondrial/cytoplasmic fraction 3.9%. Our corresponding estimates for *R. pipiens* were slightly higher: 4.3%, 7.9% and 6.6% respectively. Godula reported a surface density of $0.706 \mu\text{m}^{-1}$ rough endoplasmic reticulum and a total surface area of $7,874 \mu\text{m}^2$ per cell. Our estimates of rough ER surface area facing the cytoplasm were approximately two times larger for *R. pipiens*, with a surface density of $1.7 \mu\text{m}^2$ of RER per μm^3 cytoplasm and a total surface area of $13,600 \mu\text{m}^2$.

Fasting induced substantial morphometric changes in *R. pipiens* hepatocytes, observable using both light and electron microscopy:

(1) Average cellular volume decreased from $8,500 \mu\text{m}^3$ to $1,800 \mu\text{m}^3$. The decrease resulted mainly from a net loss of non-nuclear components, since the nuclear volume decreased less drastically, dropping from $340 \mu\text{m}^3$.

(2) The average hepatocyte/liver tissue volume fraction decreased from 80.3% to 61.7%, indicating that volume of non-hepatocyte components of the liver did not decrease as rapidly as hepatocyte volume during fasting.

(3) Mitochondrial relative volume increased from 6.6% to 25.9%. Absolute volume remained approximately constant, indicating preservation of mitochondria at the expense of other cytoplasmic components. Mitochondrial shape was altered during fasting. Mitochondrial axial ratio data indicated a significant deviation from the traditional circular cylinder model in both control and fasted animals.

(4) Lipid volume was reduced almost to zero, dropping from an initial relative volume of 7.9% to 0.01%. Absolute volume decreased correspondingly from $650 \mu\text{m}^3$ to less than $1 \mu\text{m}^3$ per hepatocyte.

(5) Glycogen volume also decreased during fasting, but detectable quantities were still present in hepatocyte cytoplasm after two months fasting. Relative volume decreased from 48.8% to 14.9%, absolute volume from $4,000$ – $240 \mu\text{m}^3$ per cell.

(6) Absolute surface area of rough endoplasmic reticulum decreased from $13,600$ to $3,000 \mu\text{m}^2$ per hepatocyte, but surface density (μm^2 of membrane per μm^3 of cytoplasm) remained approximately constant.

Organisms from different phyla have been shown to exhibit widely differing biochemical responses to starvation stress (Phillips and Hird, '77). The onset of atrophic changes caused by starvation occurs in mammalian hepatocytes after a relatively short period of starvation. Rat liver cells show a marked depletion of glycogen after 48 hours of fasting (Kugler, '67) and a decrease in size after five days (Fawcett, '55). The animals die under the stress of starvation after seven to ten days. By contrast, changes in liver structure of poikilotherms develop after much longer periods of starvation. Marked changes in hepatocyte ultrastructure are observed in starved frogs, but generally after one to two months starvation. Duveau and Piery ('73) reported survival of frogs subjected to starvation for periods lasting as long as 19 months, and Spornitz ('75) observed no significant change in ultrastructural organization or density of packing of glycogen in hepatocytes of *Xenopus laevis* even after inanition of four to five months.

Many of the ultrastructural changes observed in hepatocytes from starved frogs correspond to changes also described for starved rats. Riede et al. ('73) observed a 50% decrease in hepatocyte volume in rats subjected to chronic partial starvation for a period of six weeks. They also found (1) the nuclear-cytoplasmic volume ratio increased in favor of the nucleus, (2) the total mitochondrial volume per cell was essentially unchanged even though substantial changes in mitochondrial shape occurred, and (3) the membrane surface area of endoplasmic reticulum per hepatocyte was reduced by two-thirds following starvation.

However, there appear to be several significant differences observable at the ultrastructural level between the response of frog and mammalian hepatocytes to starvation stress. For example, an inverse relationship between the quantity of glycogen and development of smooth endoplasmic reticulum in liver cells of fasted mammals has been described by many authors (Cardell, '71; De Man and Blok, '66; Elias, '55). Our investigation failed to show a similar proliferation of smooth endoplasmic reticulum in *Rana pipiens* in response to starvation. Areas containing smooth and rough reticulum at the periphery of large "glycogen areas" were more prevalent in control animals than in the fasted group. Although free ribosomes were observed frequently in the cytoplasm in fasted animals, they were not accom-

panied by a corresponding proliferation of smooth-surfaced profiles. Our quantitative data indicate that, although rough endoplasmic reticulum decreased in absolute surface area after starvation, its surface density in the cytoplasm was not significantly altered. This suggests that its decrease was simply proportional to the decrease in total cytoplasmic volume; no corresponding increase in smooth endoplasmic reticulum was observed to support the hypothesis of selective transformation and preservation of granular reticulum as part of the agranular phase.

Differences in the apparent structure of glycogen aggregates in frogs and mammals may be related to reported differences in rates of glycogen mobilization. Although structures approximating α -rosettes were observed in frog hepatocytes, the rosettes were generally smaller than those observed in rat hepatocytes and the particles did not react uniformly to standard glycogen fixatives and stains. Following a 2-month starvation period, reduced quantities of glycogen were still present in the cell, generally in the form of β -particles. Whether these " β -particles" represent a more refractory form of glycogen or a less complex molecular stage in the glycogen degradation process cannot be determined from our results.

Our quantitative stereological data indicate an apparent selective preservation of nuclear and mitochondrial components in frog hepatocytes at the expense of the cytoplasmic ground matrix and its membranous component. Alvarez and Cowden ('66) observed that prolonged starvation of *R. pipiens* at room temperature resulted in a decreased volume of hepatocyte nuclei. The decrease in volume was not dependent on the amount of DNA, RNA or protein bound sulfhydryl groups per nucleus, but was dependent on the quantity of total nuclear protein. Our results indicate no statistically significant decrease in nuclear diameter after two months starvation. However, invaginations of the nuclear membrane were occasionally observed in starved animals, a frequent finding in some diseased or neoplastic cells (Cheville, '76). Bernhard ('69) suggests such invaginations may be associated with a regulatory mechanism which could facilitate nucleo-cytoplasmic exchange, a possible means of effecting protein transfer from the nucleus under the stress of starvation.

Riede et al. ('73) observed a significant increase in mitochondrial size in chronically

starved rats, a decrease in number of mitochondria per cell, and no significant change in absolute mitochondrial volume per cell. They suggest this indicates a functional reorganization of the chondriome in response to starvation stress. Our data, which also indicate a substantial change in mitochondrial shape but little change in absolute mitochondrial volume per cell, are consistent with this hypothesis.

Contrary to our results which showed significant glycogen depletion after two months starvation, Spornitz ('75) observed no change in the ultrastructural organization or density of packing of glycogen rosettes in hepatocytes of *Xenopus laevis* even after four to five months starvation. Nicholls et al. ('68) reported that the stage of egg development greatly influenced hepatocyte structure in female *X. laevis*, and Brachet et al. ('71) observed noticeable differences in enzymatic activity in hepatocytes of *Rana esculenta* depending on sex and on season of the year. Such observations indicate that future studies involving frog hepatocytes should be controlled for genus/species effects (which may be related to whether the species undergoes hibernation [Spornitz, '75]), sexual effects (particularly related to the female egg-laying cycle [Nicholls et al., '68; Brachet et al., '71]), seasonal effects (which may occur even in laboratory-raised animals), and nutritional state. Our data further indicate a high degree of polarity within the normal frog liver cell and a large variability among individuals obtained from the same population and raised under identical conditions. This heterogeneity argues strongly for the necessity of morphometric analyses, which allow unbiased quantitative comparisons of within and between group variances.

ACKNOWLEDGMENTS

We acknowledge Dr. A. V. Loud for reviewing the manuscript and for invaluable consultation concerning the stereological analyses. We thank Dr. George W. Nace, Director of the University of Michigan Amphibian Facility, for his guidance in proper laboratory care of our animals. We also thank T. B. Ladewski for technical assistance at all stages of the project, K. E. Guire of the University of Michigan Statistical Research Laboratory for many hours of consultation, and E. F. Stoerner and R. L. Marsh for reviewing the manuscript.

This work was supported in part by faculty Grant No. 354330 from the Horace H. Rackham School of Graduate Studies of the University of Michigan and by an award from the LSA Honors Council Max H. Cutcheon Fund, the University of Michigan.

LITERATURE CITED

- Alvarez, M. R., and R. R. Cowden 1966 Karyometric and cytophotometric study of hepatocyte nuclei of frogs exposed to cold and prolonged starvation. *Z. Zellforsch.*, 75: 240.
- Baic, D., B. E. Frye and B. G. Ladewski 1973 Intracisternal fibers in the liver cells of starved frogs. *J. Ultrastructure Res.*, 43: 478.
- Bennett, H. A., and J. H. Luft 1959 S-collidine as a basis for buffering fixatives. *J. Biophys. Biochem. Cytol.*, 6: 113.
- Bennett, T. P., and J. S. Glenn 1970 Fine structure changes in liver cells of *Rana catesbeiana* during natural metamorphosis. *Develop. Biol.*, 22: 535.
- Bennett, T. P., J. S. Glenn and H. Sheldon 1970 Changes in the fine structure of tadpole (*Rana catesbeiana*) liver during thyroxine-induced metamorphosis. *Develop. Biol.*, 22: 232.
- Bernhard, W. 1969 Ultrastructure of the cancer cell. In: *Handbook of Molecular Cytology*. A. Lima-de-Faria, ed. North-Holland Publishing Co., Amsterdam-London, p. 688.
- Brachet, J. 1969 Cytochemical changes in frog liver during gametogenesis. *Curr. Mod. Biol.*, 2: 298.
- Brachet, J., E. Brock, A. Gaudiano, G. Petti and M. Polizzi 1971 Variations biochimiques et morphologiques saisonnières dans le foie de *Rana esculenta*. *Arch. Biol. (Liege)*, 82: 25.
- Cardell, R. R., Jr. 1971 Action of metabolic hormones on the fine structure of rat liver cells. I. Effects of fasting on the ultrastructure of hepatocytes. *Am. J. Anat.*, 131: 21.
- Chalkley, H. W. 1943 Methods for the quantitative morphologic analysis of tissues. *J. Nat. Cancer Inst.*, 4: 47.
- Cheville, F. N. 1976 *Cell Pathology*. The Iowa State University Press, Ames, Iowa, 515 pp.
- Delesse, M. A. 1847 Procédé mécanique pour déterminer la composition des roches. *C. R. Acad. Sci. (Paris)*, 25: 544.
- De Man, J. C. H., and A. P. R. Block 1966 Relationship between glycogen and agranular endoplasmic reticulum in rat hepatic cells. *J. Histochem. Cytochem.*, 14: 135.
- De Robertis, E. 1938 Variaciones de la citología hepática del *Bufo arenarum* (Hensel) en el curso del año. *Rev. Soc. Biol. argent.*, 14: 145.
- Drochmans, P. 1962 Morphologie du glycogène. *J. Ultrastructure Res.*, 6: 141.
- Duveau, A., and Y. Piery 1973 Inanition prolongée et ultrastructure du foie de grenouille. *C. R. Soc. Biol. (Paris)*, 167: 491.
- Ecker, A., and R. Wiedersheim 1904 *Anatomie des Frosches*. Vol. 3. F. Vieweg und Sohn, Braunschweig, pp. 118-155.
- Elias, H. 1955 Liver Morphology. *Biol. Rev.*, 30: 263.
- Elias, H., A. Sokol and A. Lazarowitz 1954 Contributions to the geometry of sectioning. II. Circular cylinders. *Z. Wiss. Mikrosk.*, 62: 20.
- Farrar, E. 1972 Some Aspects of Carbohydrate Metabolism and its Regulation by Adrenalin and Glucagon in *Rana pipiens*. Doctoral dissertation, The University of Michigan, 184 pp.
- Fawcett, D. W. 1955 Observations on the cytology and electron microscopy of hepatic cells. *J. Nat'l. Cancer Inst.*, 15 (Suppl.): 1475.

- Floderus, S. 1944 Untersuchungen über den Bau der menschlichen Hypophyse mit besonderer Berücksichtigung der quantitativen micromorphologischen Verhältnisse. Acta Pathol. Microbiol. Scand. Suppl. 53.
- Glagoleff, A. A. 1933 On the geometrical methods of quantitative mineralogical analysis of rocks. Tr. Inst. Econ. Min. and Metal, (Moscow), 59.
- Godula, J. 1970 Quantitative investigations of cellular organelles from the liver of amphibia: *Xenopus laevis* (Daud.) and *Ambystoma mexicanum* (Cope). Acta Biol. Cracov., Ser. Zool., 13: 225.
- Haug, H. 1967 Probleme und Methoden der Strukturzählung im Schnittpräparat. In: Quantitative Methoden in der Morphologie. E. R. Weibel and H. Elias, eds. Springer, Berlin-Heidelberg-New York, p. 58.
- Jones, A. L., and D. W. Fawcett 1966 Hypertrophy of the agranular endoplasmic reticulum in hamster liver induced by phenobarbital (with a review on the functions of this organelle in liver). J. Histochem. Cytochem., 14: 215.
- Karnovsky, M. J. 1965 A formaldehyde-glutaraldehyde fixative of high osmolality for use in electron microscopy. J. Cell Biol., 27: 137A.
- Karrer, H. E. 1961 Electron microscope observations on chick embryo liver. J. Ultrastructure Res., 5: 116.
- Kugler, J. H. 1967 Correlation of the glycogen concentration in rat liver and the appearance of glycogen and agranular endoplasmic reticulum. J. Royal Microscopical Soc., 86: 285.
- Loud, A. V. 1968 A quantitative stereological description of the ultrastructure of normal rat liver parenchymal cells. J. Cell Biol., 37: 27.
- Luft, J. H. 1956 Permanganate—a new fixative for electron microscopy. J. Biophys. Biochem. Cytol., 2: 799.
- Magalhaes, M. M., and M. C. Magalhaes 1970 Ultrastructural alterations produced in rat liver by metopiron. J. Ultrastructure Res., 32: 32.
- Millonig, G., and K. R. Porter 1960 Structural elements of rat liver cells involved in glycogen metabolism. In: Proceedings of European Regional Conference on Electron Microscopy. A. L. Houwink and B. J. Spit, eds. Vol. II, p. 651.
- Millonig, G., and V. Marinozzi 1968 Fixation and embedding in electron microscopy. In: Advances in Optical and Electron Microscopy. Vol. 2. R. Barer and V. E. Cosslett, eds. Academic Press, New York.
- Minio, F., L. Lombardi and A. Gautier 1966 Mise en évidence et ultrastructure du glycogène hépatique: Influence des techniques de préparation. J. Ultrastructure Res., 16: 339.
- Mizell, S. 1965 Seasonal changes in energy reserves in the common frog, *Rana pipiens*. Gen. Comp. Physiol., 66: 251.
- Nace, G. W., D. D. Culley, M. B. Emmons, E. L. Gibbs, V. H. Hutchison and R. G. McKinnell 1974 Amphibians: Guidelines for the Breeding, Care and Management of Laboratory Animals. I.L.A.R. (NAS/NRC), Washington, D.C.
- Nicholls, T. J., B. K. Follett and P. J. Evennett 1968 The effects of oestrogens and other steroid hormones on the ultrastructure of the liver of *Xenopus laevis* Daudin. Z. Zellforschung, 90: 19.
- Pasanen, S., and P. Koskela 1974 Seasonal and age variation in the metabolism of the common frog, *Rana temporaria* L. in northern Finland. Comp. Biochem. Physiol., 47A: 635.
- Phillips, J. W., and F. J. R. Hird 1977 Gluconeogenesis in vertebrate livers. Comp. Biochem. Physiol., 57B: 127.
- Porter, K. R., and C. Bruni 1960 Fine structural changes in rat liver associated with glycogenesis and glycogenolysis. Anat. Rec., 136: 260 (Abstract).
- Revel, J. P. 1964 Electron microscopy of glycogen. J. Histochem. Cytochem., 12: 104.
- Riede, U. N., J. Hodel, Ch. V. Matt, Y. Rasser and H. P. Rohr 1973 Einfluss des Hungers auf die quantitative Cytoarchitektur der Rattenleberzelle. Beitrage zur Pathologie, 150: 246.
- Rosiwal, A. 1898 Ueber geometrische Gesteinsanalysen. Ein einfacher Weg zur ziffermassigen Feststellung des Quantitätsverhältnisses der Mineralbestandteile gemengter Gesteine. Verh. K. K. Geol. Reichsanst., (Wien), p. 143.
- Smith, C. L. 1950 Seasonal changes in blood sugar, fat body, liver glycogen, and gonads in the common frog, *Rana temporaria*. J. Exp. Biol., 26: 412.
- Snedecor, G. W. 1956 Statistical Methods. Iowa State University Press, Ames, Iowa, 435 pp.
- Spiegel, E. S., and M. Spiegel 1970 Some observations on the ultrastructure of the hepatocyte in the metamorphosing tadpole. Expt. Cell Res., 61: 103.
- Spornitz, U. M. 1975 Studies on liver of *Xenopus laevis*. I. The ultrastructure of the parenchymal cell. Anat. Embryol., 146: 245.
- Tomkeieff, S. I. 1945 Linear intercepts, areas and volumes. Nature, 155: 24.
- Underwood, E. E. 1968 Particle-size distribution. In: Quantitative Microscopy. R. T. De Hoff and F. N. Rhines, eds. McGraw-Hill Book Company, London, p. 149.
- Underwood, E. E. 1970 Quantitative Stereology. Addison-Wesley, Reading, Massachusetts, 274 pp.
- Vrensen, G. F. J. M., and C. M. A. Kuyper 1969 Involvement of rough endoplasmic reticulum and ribosomes in early stages of glycogen repletion in rat liver. J. Microscopie, 8: 599.
- Vye, M. V., and D. A. Fischman 1971 A comparative study of three methods for the ultrastructural demonstration of glycogen in thin sections. J. Cell Sci., 9: 727.
- Weibel, E. R., and R. P. Bolender 1973 Stereological techniques for electron microscopic morphometry. In: Principles and Techniques of Electron Microscopy: Biological Applications. Vol. 3. M. A. Hayat, ed. Van Nostrand Reinhold Co., New York, p. 237.

PLATE 1

EXPLANATION OF FIGURES

- 2 Low power light micrograph of 1- μ m section of frog hepatic tissue. Note absence of well-defined lobular substructure. Toluidine blue stained. \times 145.
- 3 One-micrometer toluidine blue stained section of liver tissue from summer control animal. \times 810.
- 4 Tissue from fasted summer frog prepared as in figure 3. Arrow indicates pigment cells, which are abundant in liver tissue from fasted animals. \times 810.

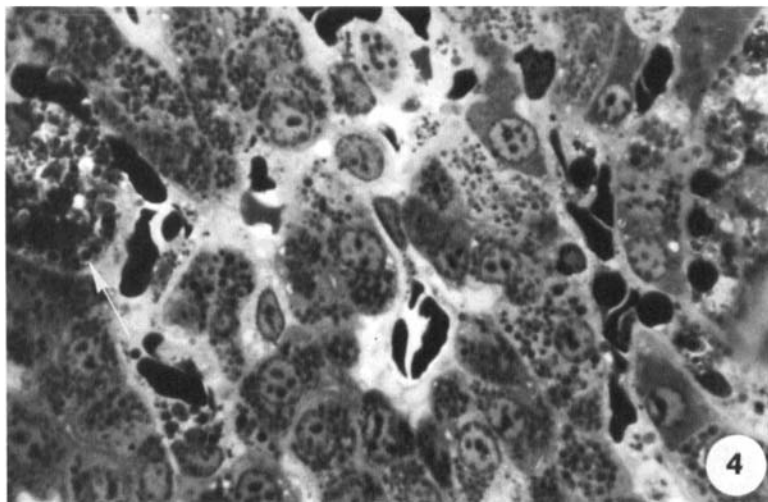
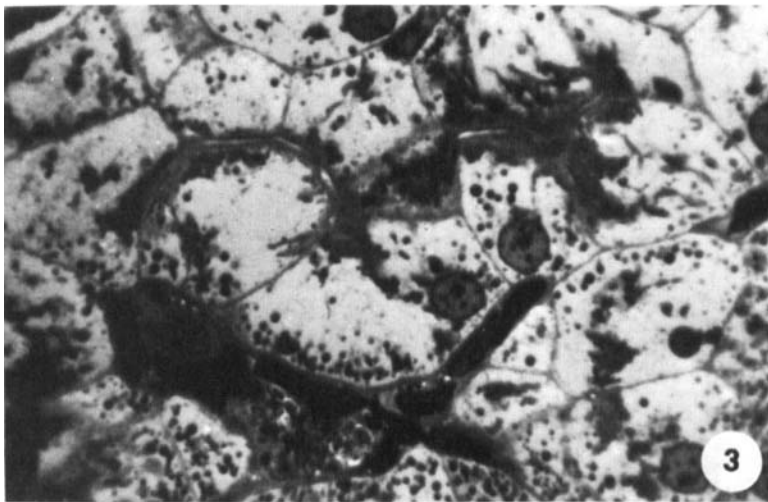
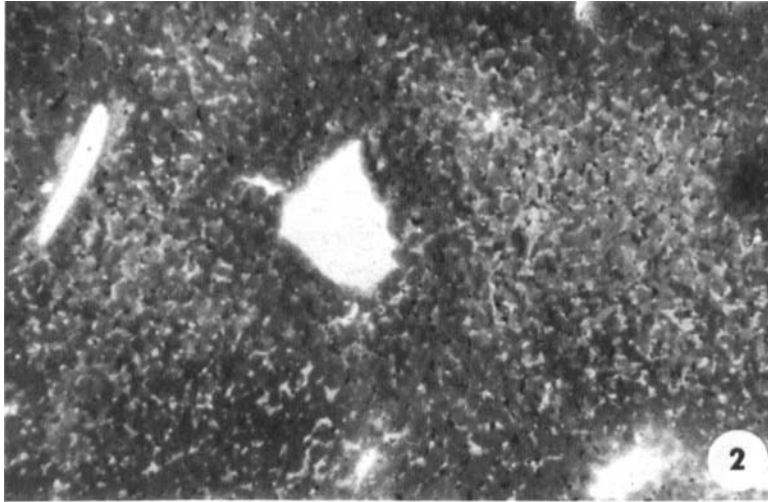


PLATE 2

EXPLANATION OF FIGURES

- 5 Summer control. Lipid is abundant in the cytoplasm near the sinusoid (arrows). Fixed in glutaraldehyde-osmium tetroxide. $\times 5,300$.
- 6 Bile canaliculus and portions of three adjacent cells from summer control tissue. Note continuity of vesicles of smooth and rough endoplasmic reticulum at the periphery of "glycogen areas." Small holes are scattered throughout the faintly-stained glycogen areas, no rosettes are visible. Fixed in glutaraldehyde-osmium tetroxide. $\times 5,100$.

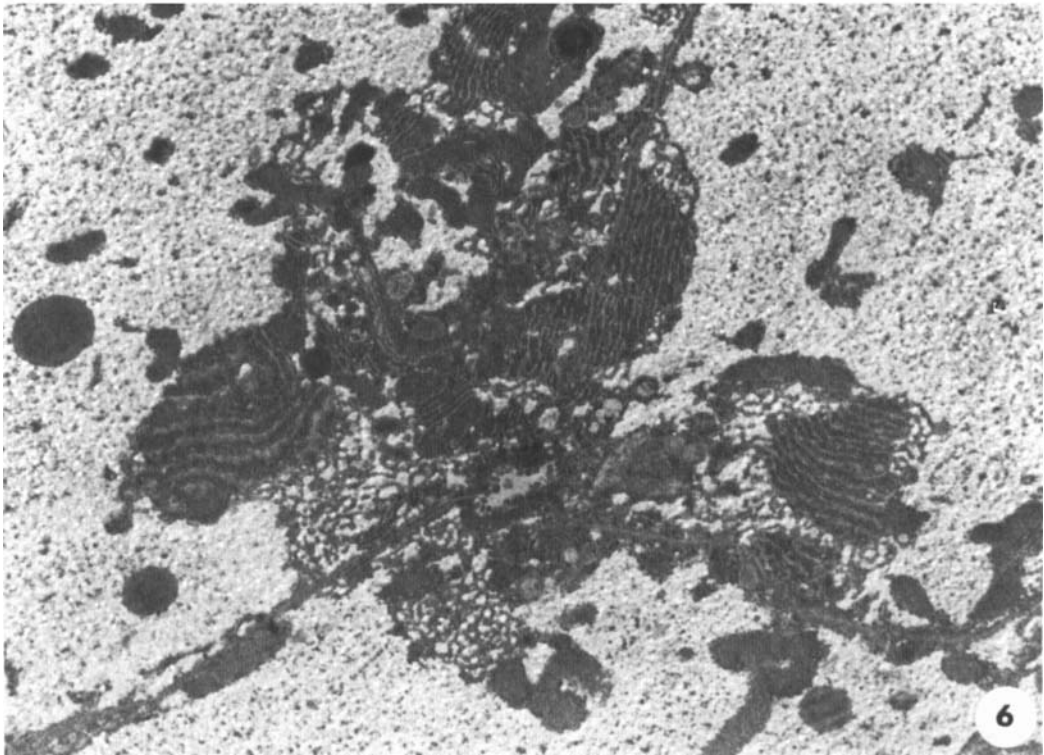
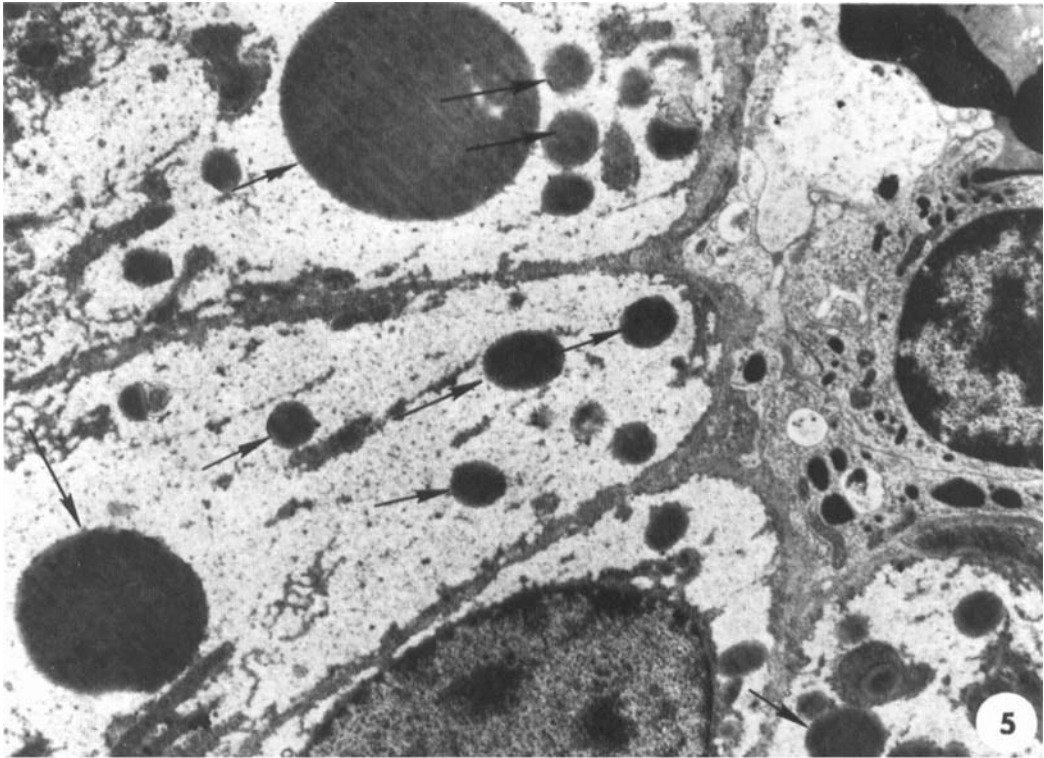


PLATE 3

EXPLANATION OF FIGURES

- 7 Summer control. High power electron micrograph showing close association of mitochondria and smooth and rough ER. Note mottled cytoplasmic ground matrix. Fixed in glutaraldehyde-osmium tetroxide. $\times 22,000$.
- 8 Summer control. High power electron micrograph of glycogen area showing interconnected glycogen particles. Fixed in glutaraldehyde-osmium tetroxide. $\times 80,000$.
- 9 Summer control. Rosettes of glycogen similar to α -configuration described in mammalian hepatocytes. Such darkly-staining aggregates were not the most frequently observed form of glycogen seen within control hepatocytes. See figures 5-8. Fixed in potassium permanganate. $\times 50,000$.

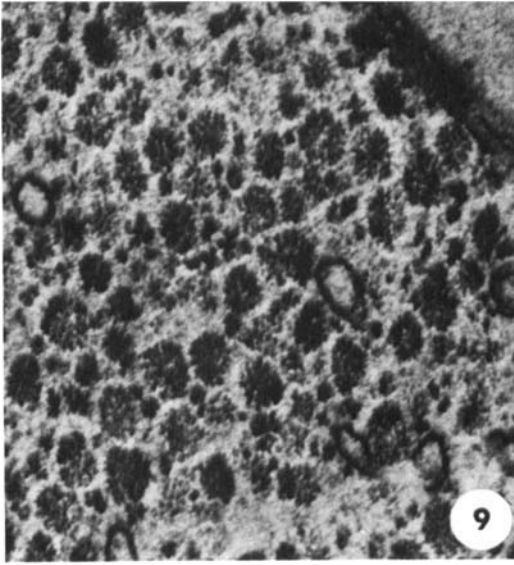
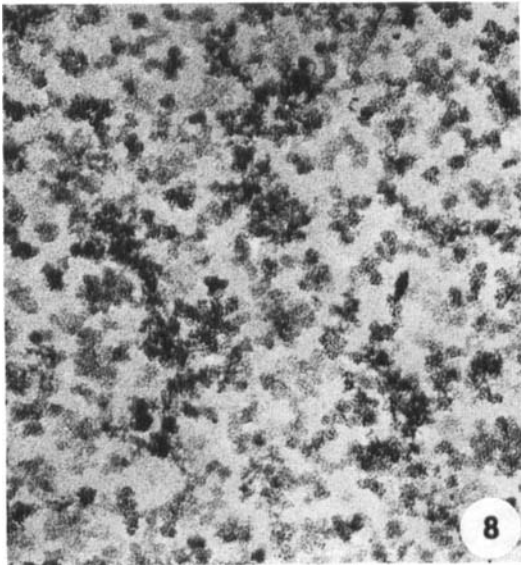
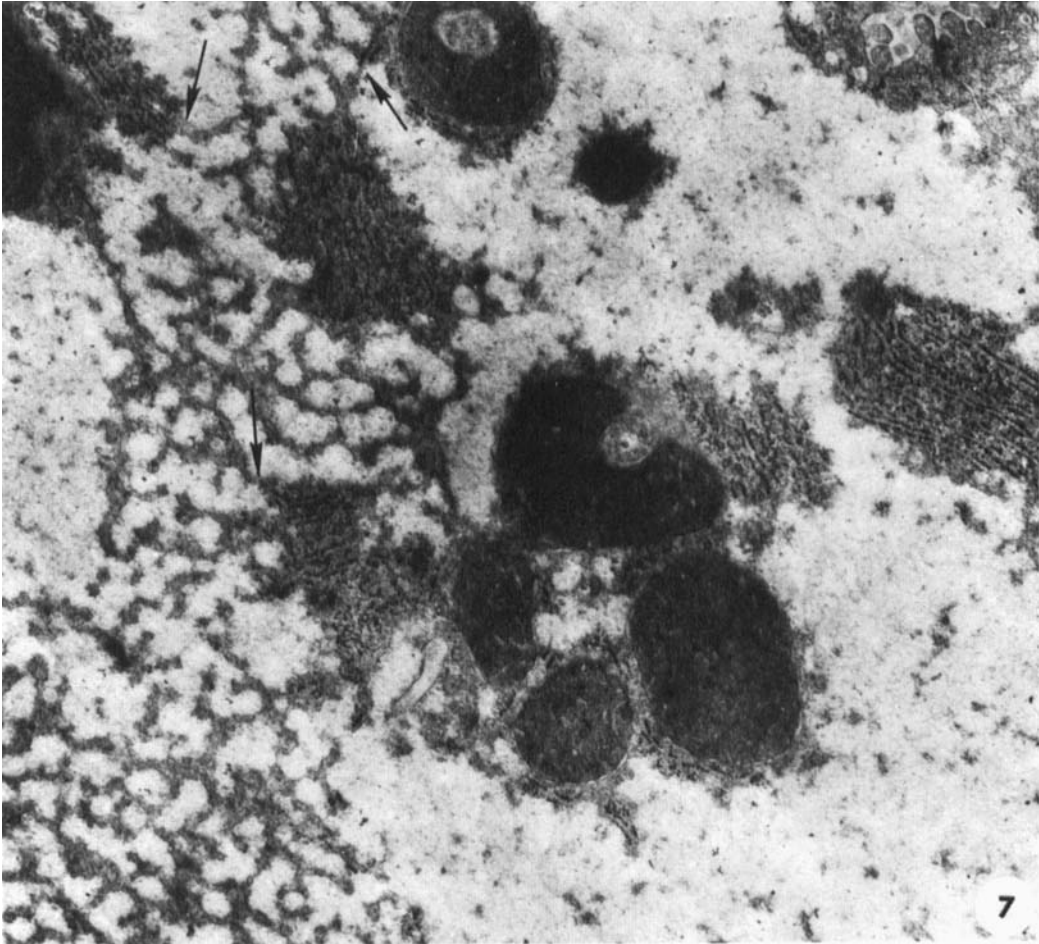


PLATE 4

EXPLANATION OF FIGURES

- 10 Permanganate-fixed tissue from summer control. Note large glycogen aggregates and stacks of endoplasmic reticulum. $\times 17,000$.
- 11 Permanganate-fixed tissue from summer fasted animal; print enlarged to same magnification as figure 10. Glycogen rosettes are not evident in the cytoplasm, and the stacks of endoplasmic reticulum are dispersed. Mitochondria appear swollen, with less well-defined cristae. $\times 17,000$.

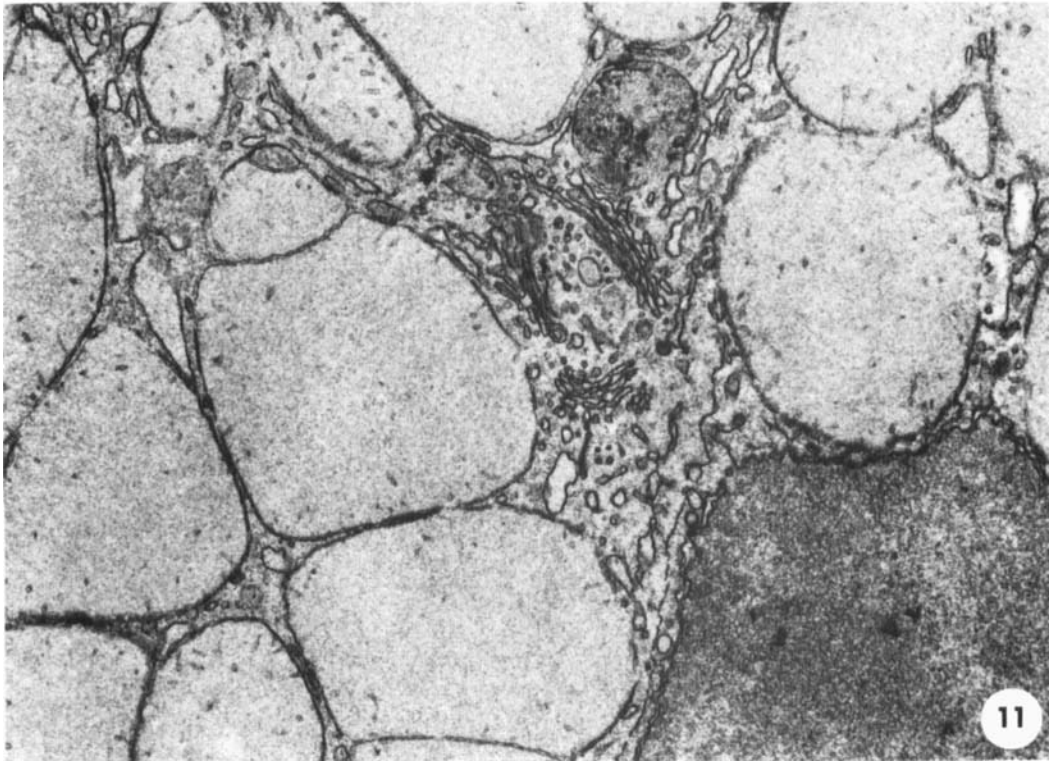
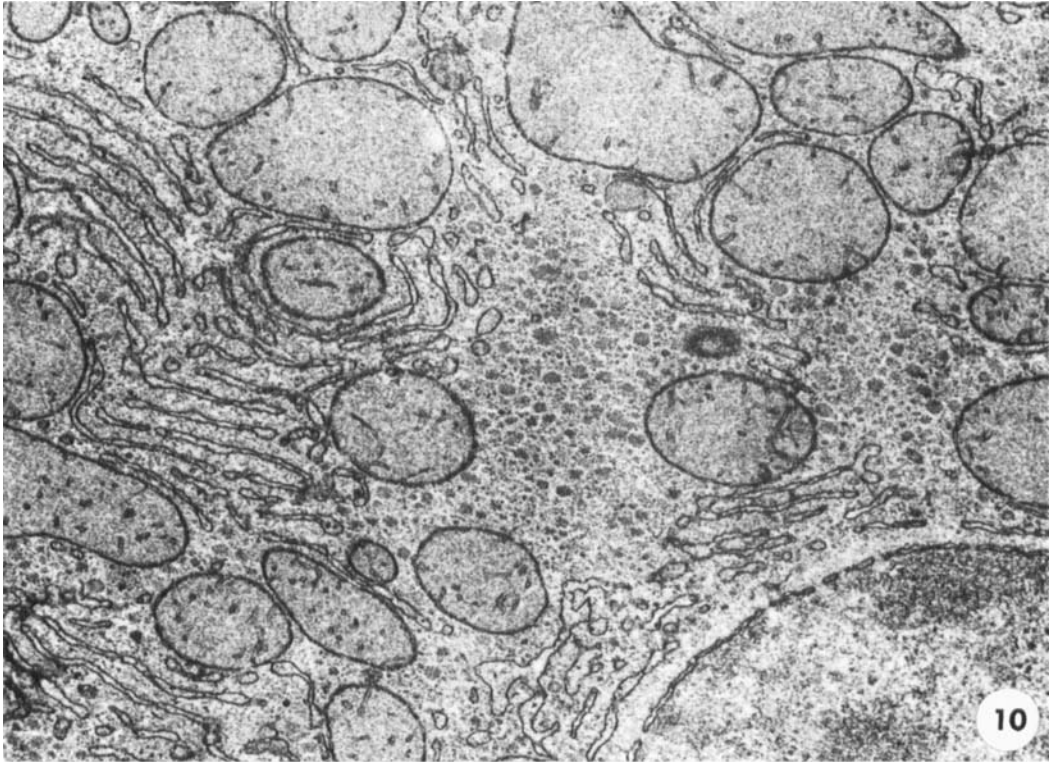


PLATE 5

EXPLANATION OF FIGURE

- 12 Fasted summer animal. Four adjacent cells bordering a sinusoid. Cell size is greatly diminished; glycogen areas are not visible. Slight invaginations are evident in the nuclear membranes of all four cells. Compare with figure 5. Fixed in glutaraldehyde-osmium tetroxide. $\times 8,000$.

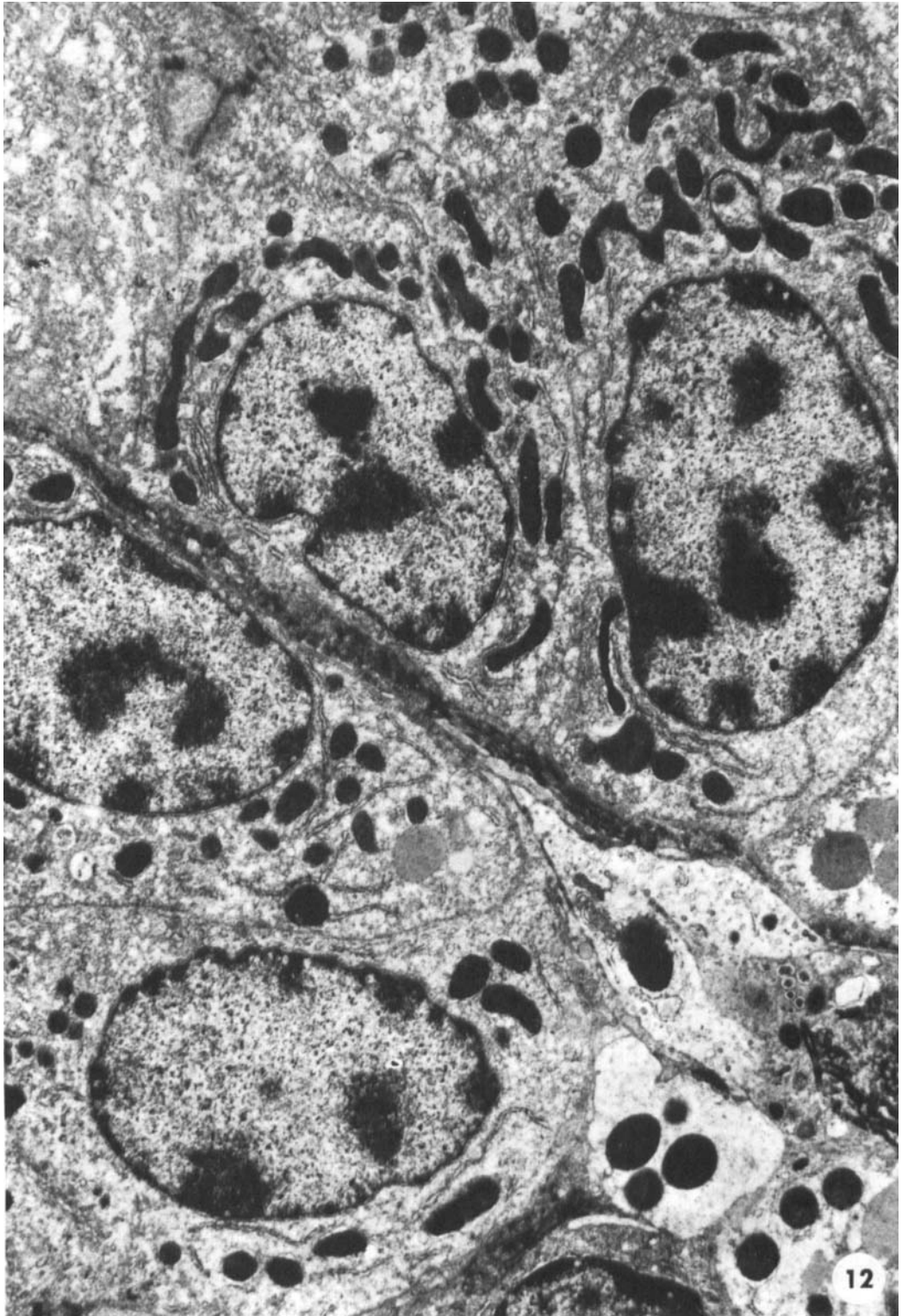


PLATE 6

EXPLANATION OF FIGURES

- 13 Hepatocyte from fasted summer animal. The stippled areas in the cytoplasm may represent the β -configuration of glycogen particles. Compare with figure 6. Fixed in glutaraldehyde-osmium tetroxide. $\times 9,600$.
- 14 Summer fasted. High power electron micrograph showing odd-shaped mitochondrion. Arrows indicate free ribosomes scattered in the cytoplasm. Fixed in glutaraldehyde-osmium tetroxide. $\times 10,000$.
- 15 Summer fasted. Glycogen particles similar to β -configuration described in mammalian hepatocytes. Compare with figures 8 and 9. Fixed in potassium permanganate. $\times 50,000$.

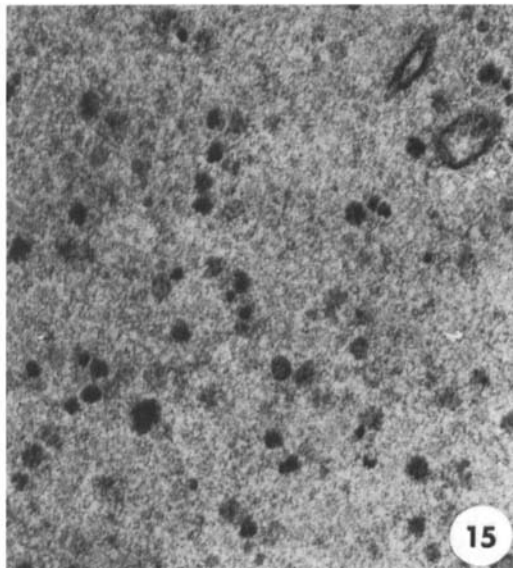
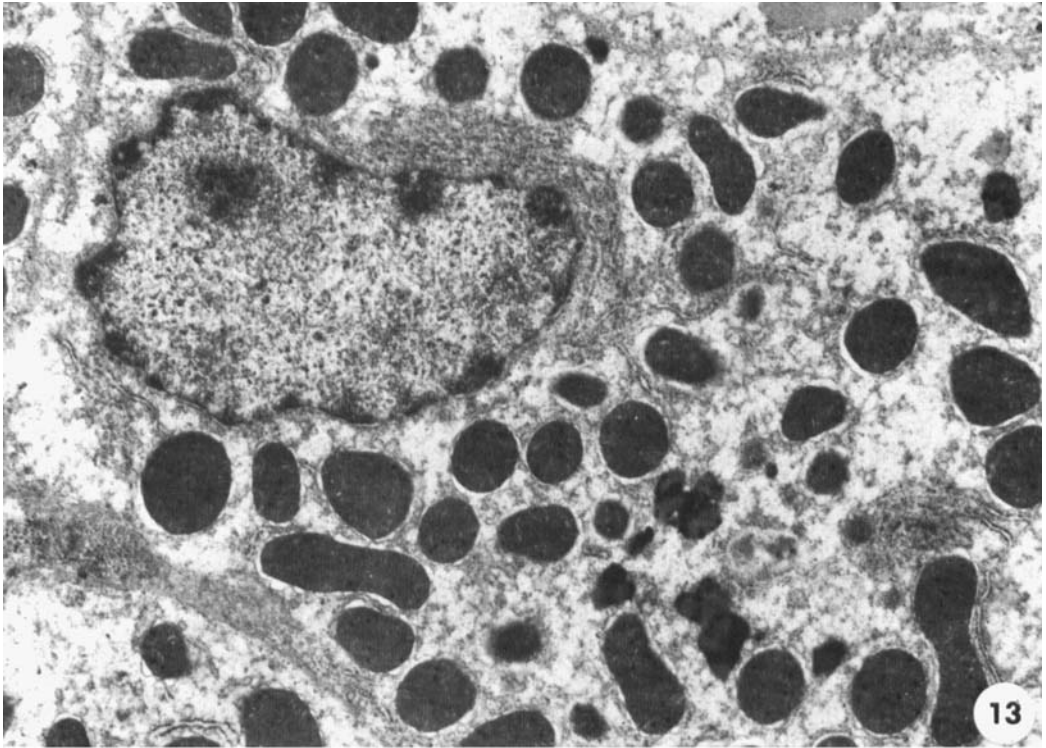


PLATE 7

EXPLANATION OF FIGURES

- 16 Summer fasted. Electron dense material was occasionally observed condensed into cross-banded fibers or sheets within the cisternae of rough endoplasmic reticulum. Fixed in glutaraldehyde-osmium tetroxide. $\times 8,700$.
- 17 Winter fasted. More advanced stages of fiber formation were observed in fasted animals from other seasons. Cisternae with well-developed cross-banded fibers have lost most of their attached ribosomes (arrows). Fixed in glutaraldehyde-osmium tetroxide. $\times 41,000$.
- 18 Summer fasted. Apparent sites of intracellular digestion (arrows). Fixed in glutaraldehyde-osmium tetroxide. $\times 15,000$.

